THE JOURNAL OF PHYSICAL CHEMISTRY B

ARTICLE

pubs.acs.org/JPCB

Structure Dependent Energy Transport: Relaxation-Assisted 2DIR Measurements and Theoretical Studies

Valeriy M. Kasyanenko,[†] Sarah L. Tesar,[†] Grigory I. Rubtsov,[‡] Alexander L. Burin,[†] and Igor V. Rubtsov[†,*]

[†]Department of Chemistry, Tulane University, New Orleans, Louisiana 70118, United States

[‡]Institute for Nuclear Research of the Russian Academy of Sciences, Moscow 117312, Russian Federation

Supporting Information

ABSTRACT: Vibrational energy relaxation and transport in a molecule that is far from thermal equilibrium can affect its chemical reactivity. Understanding the energy transport dynamics in such molecules is also important for measuring molecular structural constraints via relaxation-assisted two-dimensional infrared (RA 2DIR) spectroscopy. In this paper we investigated vibrational relaxation and energy transport in the ortho, meta, and para isomers of acetylbenzonitrile (AcPhCN) originated from excitation of the CN stretching mode. The amplitude of the cross-peak among the CN and CO stretching modes served as an indicator for the energy transport from the CN group toward the CO group. A surprisingly large difference is observed in both the lifetimes of the CN mode and in the energy transport rates for the three isomers. The anharmonic DFT calculations and energy transport modeling performed to understand the origin of the differences and to identify the main cross-peak contributors in these isomers described well the majority of the experimental results including mode excited-state lifetimes and the energy transport dynamics. The strong dependence of the energy transport on molecular structure found in this work could be useful for recognizing different isomers of various compounds via RA 2DIR spectroscopy.

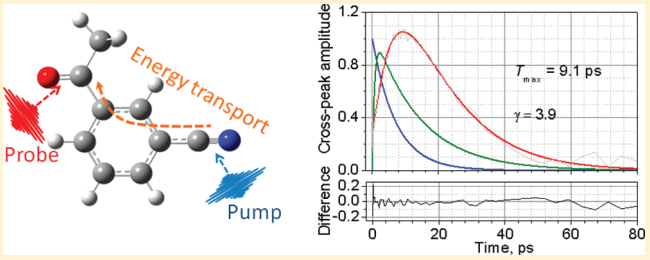

INTRODUCTION

The energy transport in molecules in condense phase occurs via the intramolecular vibrational energy redistribution (IVR) process in which the occupation numbers for several vibrational modes change at the same time.[1−4] The early stages of the IVR process, initiated by relaxation of a single high-frequency mode, occur in strongly nonequilibrium conditions with a substantial population of vibrationally excited high-frequency modes. Since the initially excited high-frequency modes are often localized, the problem of excess-energy equilibration originated from relaxation of such modes has not only a temporal but also a spatial content. Note that quasistationary approaches that use a heat diffusion equation are not applicable due to the quantum nature of the IVR process, nonequilibrium conditions, and the atomic length scale involved.

The nonlinear spectroscopic method of IR-pump and anti-Stokes-Raman-probe[5−8] has been applied to measure populations of specific vibrational modes in time following relaxation of the initially excited mode. The energy dissipation process induced by excitation of electronic states in molecules has been studied by several research groups using UV−vis−pump−IR−probe spectroscopy.[9−12]

The recently proposed relaxation assisted 2DIR approach[13,14] (RA 2DIR) of multidimensional IR spectroscopy[15−21] permits measuring the energy transport on a molecular level with a very high sensitivity. The RA 2DIR method permits amplifying by over 25-fold the amplitude of the cross peak between spatially separated vibrational modes.[22,23] The cross-peak amplification occurs due to a transport of the excess energy from the initially excited mode toward the region of localization of the probed vibrational mode. Thus, the knowledge of the energy transport dynamics on a molecular scale is essential for predicting the cross-peak amplification in RA 2DIR measurements that enhances greatly the range of accessible distances in structural measurements via 2DIR. Understanding the energy transport dynamics on a molecular level is not only fundamentally important but also useful in a variety of applications in molecular electronics.[24−27] Note however, that as opposed to the spectroscopic techniques implementing anti-Stokes-Raman-probing[5−7] the RA 2DIR method is accessing mostly not the direct population of the probed mode. As the probed mode typically has a high frequency, its population can be significant only at early stages of the energy redistribution.[28−32] It has been proven experimentally in several molecular systems that the observed cross-peak amplification comes not from excitation of the probed mode but from excitation of the lower-frequency modes that are spatially close to the probed mode and are strongly coupled to it because of their spatial overlap. This coupling does not require

Received: July 12, 2011
Revised: August 19, 2011
Published: August 22, 2011

any IR intensity for the energy accepting modes as the mechanical coupling of the spatially overlapping modes provides a substantial mode interaction,[22,33,34] although an electric coupling contribution could be important for IR active energy accepting modes as well.[35]

In this work we investigated the energy transport in three isomers of acetylbenzonitrile (AcPhCN), ortho, meta, and para, originated from excitation of the CN stretching mode. The C≡N/C═O cross peak was measured in all three isomers using the RA 2DIR method. As the phenyl ring can be thought as having vibrational states totally delocalized over the ring, similar energy transport rates into the o, m, or p positions with respect to the CN group could be expected. The experiment demonstrated large differences in the energy transport dynamics between the three isomers. The recently developed theory[36] was applied to compute vibrational relaxation times of all modes and the energy transport dynamics in the three isomers. The modeling used the third-order anharmonic coupling constants obtained via DFT calculations with the Gaussian 09 software[37] and was capable to reproduce the majority of the characteristic features observed in the experiment.

EXPERIMENTAL DETAILS

2DIR Spectrometer. The details of the dual-frequency 2DIR setup with heterodyned detection have been reported in ref 22, 38, and 39 Briefly, the laser pulses at 804 nm and 44 fs in duration produced by a Ti:sapphire oscillator/regenerative amplifier tandem (Vitesse/UPS-Legend, Coherent Inc.) were used to pump two in-house built optical parametric amplifiers (OPA), which generate two sets of near-IR Signal and Idler pulses. Two sets of mid-IR pulses, independently tunable from 2.5 to 10 μm, were produced from the Signal and Idler pulses via difference-frequency generation (DFG) performed in two 2 mm thick $AgGaS_2$ crystals. Each mid-IR beam of ca. 3 μJ/pulse energy was split into two parts. Three beams were focused onto the sample in the phase-matching geometry, and the forth beam was used as a local oscillator (LO). The delays between the first and second and the second and the third pulses are referred to as the dephasing time, τ, and the waiting time, T, respectively. Linear-motor-driven translation stages equipped with hollow retro-reflectors were used to control the time delays between the IR pulses. The positions of all the stages were measured accurately with an external interferometric in-house built system, which uses a HeNe laser and Michelson interferometer having small glass retro-reflectors attached to the back side of the hollow retro-reflectors as its moving arms and mirrors in the stationary arms.

A third order signal generated in the sample in the phase matching direction $(-k_1 + k_2 + k_3)$ was focused onto a HgCdTe detector (Infrared Associates Inc.), where it was mixed with the local oscillator pulse, delayed by a time delay, t. The first two pulses, k_1 and k_2, originated from the same OPA and had therefore the same spectra; the third pulse, k_3, and LO pulses originated from another OPA and could have a different spectrum from that of the k_1 and k_2 pulses.

Relaxation-Assisted 2DIR Measurements. The waiting time, T, dependence of the cross-peak amplitude was measured by acquiring 2DIR (t, T) data sets, keeping the dephasing time (τ) constant, typically at 200 fs.[13] The (t, T) data sets were then Fourier transformed along the t direction and presented as a set of one-dimensional ω_t spectra at various T values. The experimental conditions for acquiring (t, T) data sets were selected so that only a single peak along ω_τ was observed in the respective 2DIR (ω_t, ω_τ) spectrum. The cross-peak amplitude at each T delay was determined by integrating the ω_t absolute-value peak in the vicinity of its maximum and subtracting the integrated and normalized background. The resulting cross-peak amplitudes were plotted as a function of the waiting time, T.

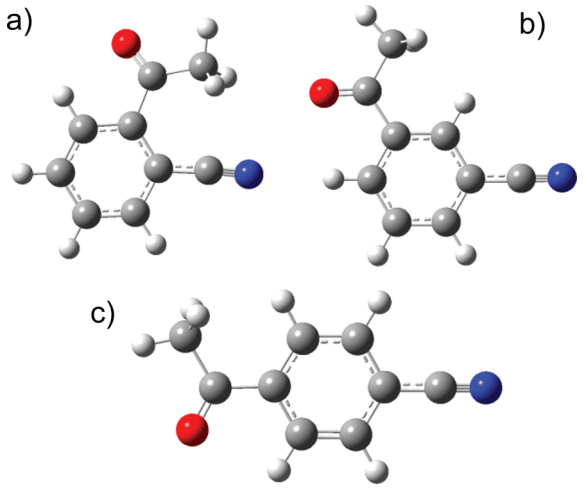

Figure 1. Structures of the ortho (a), meta (b), and para (c) isomers of AcPhCN.

Infrared Pump−Probe Measurements. Dual-frequency IR pump−probe measurements were performed using two IR pulses. The probe pulses were ca. 10-fold weaker than the pump pulses. After passing through the sample the probe beam was directed to a monochromator (Triax-190, Jobin-Yvon Co.) with a HgCdTe detector attached. The spectral resolution in the transient spectra reported is ca. 1.5 cm^{-1}. The instrument response in the transient kinetic measurement was ca. 120 fs. For each data set reported here, including transient kinetics and transient spectra, ca. 10 individual scans were averaged.

Sample Preparation. The ortho (Key Organics Ltd.), meta (Pfaltz & Bauer, Inc.), and para (Aldrich) isomers of acetylbenzonitrile (AcPhCN; Figure 1) were dissolved in chloroform. For the laser experiments the 50 mM solution of each isomer was placed in a sample cell made of two 1 mm BaF_2 wafers and a 50 μm thick Teflon spacer. All experiments were performed at room temperature, 23.5 ± 0.7 °C. To ensure that samples of the AcPhCN isomers are not degrading during the experiment, they were checked before and after the experiments by measuring their linear absorption spectra; no measurable changes were observed.

DFT Calculations. Density functional theory (DFT) anharmonic calculations were performed for each isomer using the laboratory cluster and the Gaussian 09 software package.[37] All calculations were done using the B3LYP functional and a range of basis sets, including 6-31G(d, p), 6-311G(d, p), 6-311G+(d, p), and 6-311G++(d, p), in vacuum and in chloroform solvent represented with a polarizable continuous model (PCM). A tight optimization criterion and ultrafine integration grid were used. A combination of best fits to the linear absorption spectra and nonnegative (real) anharmonic frequencies were found using the 6-311G+(d, p) basis set in vacuum and all results in this paper are presented for these conditions.

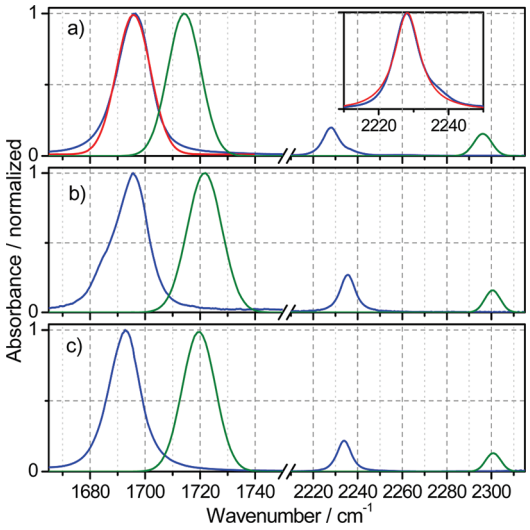

Figure 2. Normalized experimental linear absorption (blue) and DFT computed anharmonic (green) spectra for (a) *ortho*-, (b) *meta*-, and (c) *para*-AcPhCN. The computed spectra were obtained by broadening of the calculated bar spectra using a Gaussian line shape function with the respective width of 14.6 and 8.0 cm^{-1} for the CO and CN peaks, respectively. The best fits for the CO peak with Gaussian function (a) and for the CN peak with Lorentzian function (a) inset are shown with red lines.

Table 1. Experimental and Computed Anharmonic Central Frequencies (all in cm^{-1}) for the CN and CO Stretching Modes in *o*-, *m*-, and *p*-AcPhCN

	CN stretch		CO stretch	
	exp	calc[a]	exp	calc[a]
o-AcPhCN	2227.9	2296/2290.7	1696.6	1715/1693
m-AcPhCN	2235.6	2300/2294.6	1695.6	1722/1698.5
p-AcPhCN	2233.7	2301/2291.7	1692.7	1720/1695.9

[a] Anharmonic frequencies calculated in vacuum/in chloroform are shown.

RESULTS

Linear Absorption Spectra. Linear absorption spectra of the ortho, meta, and para isomers of AcPhCN are shown in Figure 2 (blue lines). The central frequencies of the CO stretching modes are very similar for the three AcPhCN isomers (Figure 2 and Table 1). The central CN frequencies for the meta and para compounds are very similar, while for the ortho isomer the CN frequency is lower by ca. 6 cm^{-1}, indicating that it is affected by the closeness of the acetyl group. The absorption spectra computed via DFT anharmonic calculations in vacuum (Figure 2, green lines) match reasonably the peak frequencies as well as the transition intensities, although all computed frequencies are larger by a factor of 1.02−1.03 and the intensities of the CN stretching modes are uniformly underestimated in calculations by a factor of 1.4 relative to that of the CO mode. Note that in each theoretical spectrum in Figure 2, obtained by broadening of the bar spectrum, the areas under the peaks are proportional to the computed IR intensities.

The experimental and computed CN and CO central frequencies for all three isomers are summarized in Table 1. The CN absorption peaks can be fit well with a Lorentzian function (Figure 2a, inset), whereas the CO transitions can be fit better with a Gaussian function (Figure 2a). Overall, the CN and CO vibrational modes of the three compounds bear high similarity.

Relaxation-Assisted 2DIR Measurements. Figure 3 shows the waiting time, T, dependence of the cross-peak amplitudes obtained from the 2DIR (t, T) measurements for the cross-peaks between CN and CO modes for *o*-, *m*-, and *p*-AcPhCN. In these experiments the k_1 and k_2 laser pulses were centered at 2242 cm^{-1} and k_3 was centered at 1681 cm^{-1} for ortho and meta and at 1695 cm^{-1} for para isomers, respectively. All measurements were done at the magic-angle polarization conditions. The cross-peak amplitude is nonzero at $T \approx 0$ indicating that the direct CN-CO coupling is substantial. The amplitude of the cross-peak for each compound grows at larger T values and reaches its maximum at 5.4, 9.1, and 10.1 ps for the *o*-, *m*-, and *p*-AcPhCN isomers, respectively. The growth of the signals is due to the energy transport from the initially excited mode (CN) to the site where the probed mode (CO) is located.[14] The decay tail of the curves is associated with two processes: energy equilibration in the molecule toward a more uniform distribution among different modes and cooling via dissipation into the solvent.[23,40,41] All three dependences show a substantial growth of the cross-peak amplitude; the amplification factors, γ, were measured at 12.5, 3.9, and 4.5 for the ortho, meta, and para isomers, respectively (Table 2). The amplification factor is determined as a ratio of the cross peak amplitude at the maximum and that at $T = 0$. Large amplification factors indicate the influence of the energy transport in the molecule on the cross-peaks. Interestingly, the T_{max} time correlates with the number of bonds separating the CN and CO groups or with the through space distance between these groups (Table 2). It is common that larger amplification factors are observed for larger intermode distances, especially when these distances are substantial.[22,23,42] For example, the amplification coefficients for the CN/amide-I and CN/CO cross-peaks in the organic molecule 4-(4-oxo-piperidine-1-carbonyl)-benzonitrile (PBN) with the distances between CN−amide and CN−CO groups of 6.5 and 11 Å were found to be 4.3 and 18, respectively.[23,43] Interestingly, the data for the ortho, meta, and para isomers show no correlation of γ with distance. The bigger value of the amplification factor is observed for *o*-AcPhCN where the distance between the CN and CO vibrational modes is the shortest of all three isomers. Note that while the initial ($T = 0$) cross-peak amplitude is determined by the direct CN/CO coupling it is difficult to determine experimentally the CN/CO off-diagonal anharmonicity, $\Delta_{CN/CO}$, as its value is very small for all three isomers (Table 2).

Lifetimes of the CN and CO Modes. A finite CN lifetime affects significantly the experimental T_{max} and γ values for the CN/CO cross peak by providing a delay for the energy release. Significantly differing lifetimes in different isomers, if found, will also indicate variations in the coupling pattern in the isomers and provide an important data for testing theoretical models for vibrational relaxation and energy transport (vide infra). The lifetimes of the CN and CO modes were measured using transient pump−probe spectroscopy with the magic angle between the polarizations of the pump and probe pulses. Figure 4 shows the diagonal transient spectra measured in *o*-AcPhCN for the CN (a) and CO (b) modes (transient spectra for other isomers are given in the Supporting Information, Figure S1). At time delays smaller than 3−5 ps both transient spectra are dominated by a negative $0 \rightarrow 1$ transition that matches the peak

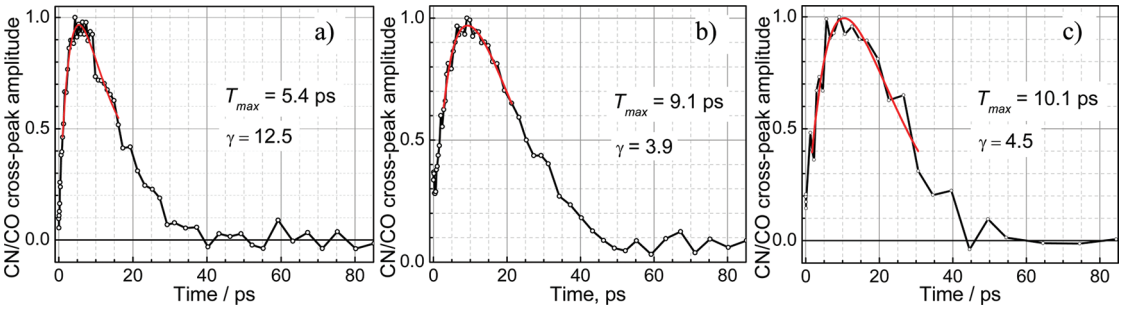

Figure 3. Normalized CN/CO cross-peak amplitude measured as a function of the waiting time, T, for the (a) ortho, (b) meta, and (c) para isomers of AcPhCN. The red lines are the fits with a two-exponential function performed in the vicinity of the maximum which were used for determining the time delay of the peak, T_{max}. The respective values of T_{max} and γ are shown in the graphs. For all three sets the dephasing times τ was 133 fs.

Table 2. Experimental and Theoretically Calculated Lifetimes, Energy Transport Times (T_{max}), Amplification Factors ($\gamma_{CN/CO}$), Anharmonicity Values, and CN/CO Distances for Three AcPhCN Isomers

	o-AcPhCN		m-AcPhCN		p-AcPhCN	
	exp	calc	exp	calc	exp	Calc
CN lifetime, ps	3.4 ± 0.2	1.2	7.1 ± 0.3	3.8	7.2 ± 0.2	3.4
CO lifetime, ps	1.8 ± 0.2	1.05	1.2 ± 0.2	1.9	2.1 ± 0.2	2.0
T_{max}(CN/CO), ps	5.4 ± 0.5	2.9	9.1 ± 0.7	6.7	10.1 ± 1	6.9
$\gamma_{CN/CO}$	12.5 ± 2	16	3.9 ± 0.4	19	4.5 ± 0.6	38
$\Delta_{CN/CN}$, cm^{-1}	−22.7	−22.8	−22.3	−22.8	−23.7	−22.8
$\Delta_{CO/CO}$, cm^{-1}	−20.0	−19.5	−22.0	−19.2	−20.0	−19.1
$\Delta_{CN/CO}$, cm^{-1}		−0.047		0.069		−0.036
through bond (through space) CN−CO distance, Å	4.4 (3.1)		5.7 (5.0)		7.1 (5.7)	

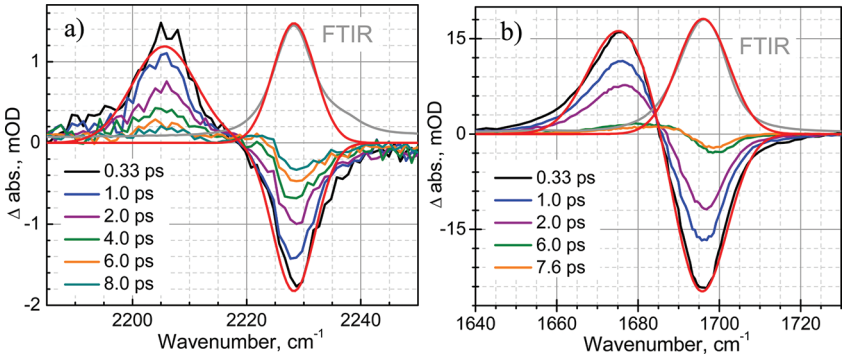

Figure 4. Diagonal pump−probe spectra for *o*-AcPhCN measured at different delay times (see insert) along with the linear absorption spectrum (gray) for the CN (a) and CO (b) modes. Red line shows the fit of the CN transient spectrum on graph a) together with the linear spectrum using Gaussian lineshapes. The transient spectra fitted with the $R(\omega) = A\{(\kappa/\sigma_{12})\exp(-[(\omega-\omega_{12})^2/\sigma_{12}{}^2] - (1/\sigma_{01})\exp(-[(\omega-\omega_{01})^2/\sigma_{01}{}^2)]\}$ function, resulted in the following parameters. For the CN diagonal signal: ω_{01} = 2228.2 cm^{-1}, σ_{01} = 5.2 cm^{-1}, ω_{12} = 2205.5 cm^{-1}, σ_{12} = 8.0 cm^{-1}, κ = 1. For the CO diagonal signal: ω_{01} = 1696.5 cm^{-1}, σ_{01} = 9.0 cm^{-1}, ω_{12} = 1676.5 cm^{-1}, σ_{12} = 11.0 cm^{-1}, and κ = 0.79.

in the linear absorption spectrum and a positive 1 → 2 transition, which is broader by a factor of 1.35 for both CN and CO modes. The 0 → 1 and 1 → 2 transitions peak at ca. 2229 and 2206 cm^{-1} for the CN mode (Figure 4a) and ca. 1696 and 1676 cm^{-1} for the CO mode (Figure 4b), resulting in the apparent diagonal CN and CO anharmonicities of ca. 23 and 20 cm^{-1}, respectively (Table 2).

At larger delay times the diagonal signal changes significantly, which is most apparent in a shift of the zero-crossing frequency, which increases at delays larger than ca. 3 ps (Figure 4). At even larger delays the transient CN spectra show an additional positive peak at ca. 2222 cm^{-1} (Figure 4a), which originates from the $|X\rangle \rightarrow |X + CN\rangle$ transitions, where X stands for the modes populated via vibrational relaxation from the CN mode; the mean coupling between the CN and X modes ($\Delta_{X/CN}$) is substantial indicated by a significance of the contribution at 2222 cm^{-1}. Notice that although the absolute transient amplitude at ca. 2222 cm^{-1} is small, the changes of the transient spectrum shape with time indicate clearly the presence of the peak. The growth of the peak at ca. 2222 cm^{-1} can be seen already at 4 ps delay (Figure 4a).

dx.doi.org/10.1021/jp2066315 |*J. Phys. Chem. B* 2011, 115, 11063–11073

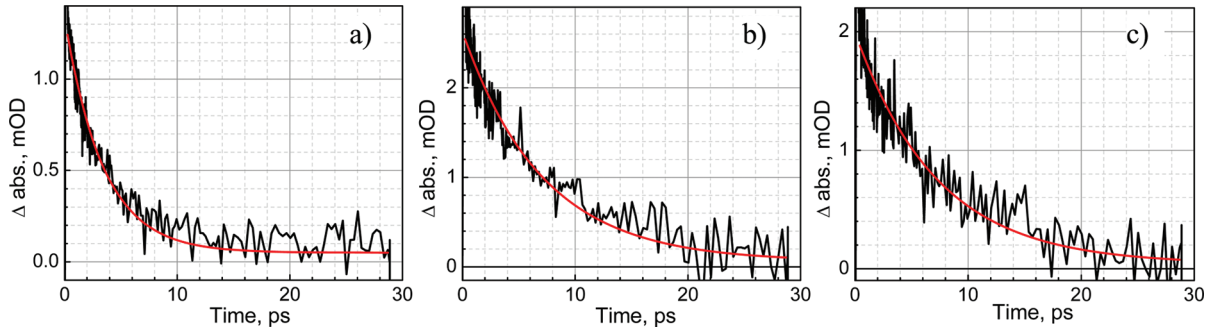

Figure 5. Transient kinetics of the CN stretching mode for (a) *ortho*-, (b) *meta*-, and (c) *para*-AcPhCN measured at 1 → 2 transition frequency (at 2206, 2214, and 2210 cm^{-1}, respectively) at magic angle conditions. The red curves show the fits with one-exponential decay function (see Table 2).

A similar effect is seen in the CO diagonal transient spectra; an additional peak at ca. 1688 cm^{-1} is clear in the spectra at 6.0 and 7.6 ps delays (Figure 4b).

The kinetics at frequency that is close to the maximum of the 1 → 2 transition were selected for the lifetime assessment (Figure 5). The fit with a single-exponential function resulted in the lifetimes of the CN mode of 3.4 ± 0.2, 7.1 ± 0.3, and 7.2 ± 0.2 ps for the ortho, meta, and para isomers, respectively (Figure 5 and Table 2). Interestingly, the lifetime of the CN mode in the ortho isomer is over 2-fold shorter than those in the meta and para compounds. This difference can be assigned to additional (and/or more efficient) relaxation channels in the ortho compound due to the closeness of the acetyl group.

Fitting of the transient spectra with an $R(\omega)$ function (Figure 4 caption) resulted in the CN diagonal anharmonicities of 22.7 ± 2, 22.3 ± 2, and 23.7 ± 2 cm^{-1} for the ortho, meta, and para isomers, respectively. The measured diagonal anharmonicities are close to those obtained via DFT anharmonic calculations, which were 22.8 cm^{-1} for all three isomers.

The fit of the 1 → 2 kinetics for the CO transition measured at 1677, 1673, and 1673 cm^{-1} with a single-exponential function (not shown) resulted in the CO lifetimes of 1.8 ± 0.2, 1.2 ± 0.2, and 2.1 ± 0.2 ps for the ortho, meta, and para isomers, respectively (Table 2). The early time delay transient CO spectra were fitted with the $R(\omega)$ function that resulted in the CO diagonal anharmonicities of 20 ± 2, 22 ± 2, and 20 ± 2 cm^{-1} for the ortho, meta, and para isomers, respectively (Figure 4b). These results are in a reasonable agreement with the anharmonicities obtained via DFT anharmonic calculations, which were found to be 19.5, 19.2, and 19.1 cm^{-1} for the ortho, meta, and para isomers, respectively (Table 2).

DISCUSSION

Correlation of T_{max} with Distance. A clear correlation between the energy transport time, T_{max}, and the intermode distance is observed for the three isomers (Table 2). The through-bond distances between CN and CO groups among ortho−meta and meta−para isomers differ by a single CC bond in the phenyl ring. Note however, that from a vibrational viewpoint the "ideal" phenyl ring having equivalent CC and CH bonds can be described as sets of vibrational modes fully delocalized over the ring. The observed correlation suggests that the vibrational modes of the phenyl ring are not fully delocalized over the ring in the AcPhCN isomers; the acetyl and cyano groups perturb the phenyl ring sufficiently to prevent the full delocalization. This perturbation can occur via changing the electronic distribution in the phenyl ring, which leads to changes in bond orders in the ring and consequently to changes in the mode delocalization. Vibrational coupling of the modes in the ring with those of the acetyl and cyano substituents can also affect the delocalization. Due to this perturbation, it is important for the energy transport from which position, o, m, or p the excess energy enters the phenyl ring, as observed experimentally. Thus we conclude that the phenyl ring in these experiments behaves not as a single unit with totally delocalized vibrations but rather as a set of individual CC bonds with only partially delocalized vibrational modes.

Different CN-mode lifetimes in the AcPhCN isomers affect differently the respective T-delay dependences as well as the T_{max} values. Deconvolution of the experimental data with the exponential function decaying with the CN lifetime permits isolating the true energy transport dynamics that is free from the influence of the finite lifetime of the initially excited mode. The fit of the convolution of the two-exponential (rise and decay) function with the exponentially decaying function, representing the CN excited state dynamics (lifetime), was performed (Figure 6, red lines). The deconvoluted functions (green lines) show the cross-peak amplitudes which would be observed if the lifetime of the initially excited CN mode is infinitely short. The characteristic times obtained from the deconvolution differ significantly for different compounds (Figure 6 caption). The rise time for *o*-AcPhCN is close to zero (<0.1 ps), which shows that the cross peak grows concomitantly with the CN decay. This suggests that there are many modes contributing strongly to the cross peak that are populated directly from the CN relaxation in the *o*-AcPhCN isomer. The rise times in *m*- and *p*-AcPhCN (0.7 ± 0.4 and 1.0 ± 0.3 ps) are substantially larger than that in *o*-AcPhCN indicating that one or more energy transfer (relaxation) steps are required to enhance the respective cross peaks.

Interestingly, the transport rates calculated as the through-bond distance divided by the true energy transport time are essentially the same in the meta and para isomers taking the values of 2.6 Å/ps. As we will see from the modeling, the similarity of the transport in *m*- and *p*-AcPhCN can be well described by the IVR process occurring via anharmonic interactions without evoking the ballistic energy propagation, which would proceed with a constant speed. Therefore, we consider the similarity of the energy propagation speeds in *m*- and *p*-AcPhCN as accidental rather than indicative of a ballistic contribution to the energy transport.[9,44,45] Surprisingly, the energy transport rate for meta and para isomers is somewhat smaller than the transport rates in PBN, which were 4.3 and 3.6 Å/ps for the CN/amide-I

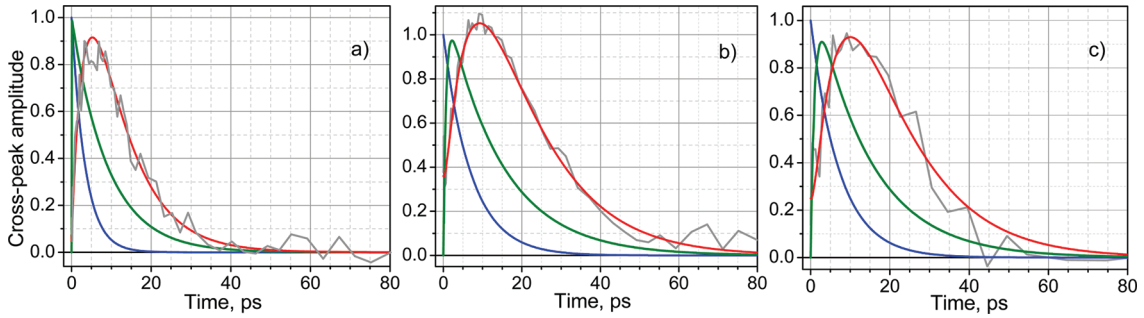

Figure 6. Results of the deconvolution of the experimental data shown in Figure 3. The red curves are the convolutions of the two-exponential (rise-decay) functions (green) with an exponential decay function (blue) with the decay times of 3.4 (a), 7.1 (b), and 7.2 ps (c). The obtained deconvoluted functions (green) have characteristic times of <0.1 and 9 ± 1 (a); 0.7 ± 0.4 and 14 ± 1 ps (b); and 1.0 ± 0.3 and 14 ± 1 ps (c). They reach maximum at (a) <0.2, (b) 2.2, and (c) 2.8 ps, respectively.

Table 3. Anharmonicities of Selected Vibrational Modes That Are Coupled Strongest to the CO Stretching Mode and Mean CO/X Anharmonicities for Selected Frequency Ranges of Modes X (all in cm^{-1}) for the Three Isomers

	o-AcPhCN	*m*-AcPhCN	*p*-AcPhCN
modes with largest $\Delta_{CO/X}$; the mode number (in front) and ω_X (in brackets)	21: −4.147(953.6)	21: −4.252(942.1)	21: −4.668(942.6)
	24: −2.1(1020.6)	14: −3.006(608)	4: −2.455(158.44)
	13: −1.68(590.3)	4: −2.33(147.2)	25: −2.374(1026.5)
	10: −1.517(450.2)	25: −2.319(1026.2)	11: −2.214(538.2)
	14: −1.35(598.2)	30: −1.579(1253.2)	34: −1.827(1407)
	39: −1.016(1591.8)	26: −1.183(1084.6)	15: −1.452(642.4)
	30: −0.819(1228.2)	13: −1.18(568.7)	26: −1.441(1069.3)
mean $\Delta_{CO/X}$ and mean $\lvert\Delta_{CO/X}\rvert$ for ω_X in different ranges:			
1000−1650 cm^{-1}	−0.451/0.612	−0.722/0.735	−0.816/0.816
600−1000 cm^{-1}	−0.712/0.687	−0.810/0.937	−0.837/0.837
300−600 cm^{-1}	−0.539/0.733	−0.563/0.659	−0.587/0.601
<300 cm^{-1}	0.121[a]/0.327	−0.447/0.538	−0.558/0.597
$\Delta\nu_{temp}$ [b], cm^{-1}	+0.08	−0.16	−0.20

[a] The mean anharmonicity is positive for ω_X modes ≤564 cm^{-1}. [b] The CO mode frequency shift corresponding to the temperature increase of 10 K with respect to the room temperature.

and CN/CO mode pairs respectively.[13,23,42] The decay times of the deconvoluted functions (9 ± 1, 14 ± 1, and 14 ± 1 ps in the o, m, and p isomers, respectively) show that the cross peak diminishes significantly faster in the ortho isomer. Does it mean that the ortho isomer cools down faster by transferring the excess energy to the solvent? We will discuss this issue in the next section.

Amplification Factor Variations. The amplification factors (γ) and the whole waiting-time dependences can be compared for the three isomers. The factors affecting the γ value include the direct coupling strength ($\Delta_{CN/CO}$), the existence of modes strongly coupled to the probed mode (CO), the energy transport time to and the overall cooling time of such modes, the lifetime of the initially excited mode, and the overall cooling time of the whole molecule. The CN/CO anharmonicities for the three isomers differ by less than a factor of 2 in absolute value (Table 2), but the anharmonicity for *o*-AcPhCN is not the smallest of all. The energy transport time correlates with the CN-CO distance. Shorter CN lifetime in *o*-AcPhCN indeed causes an increase in γ, but the increase, tested by convoluting a typical rising and decaying dynamics with 7.2 and 3.4 ps lifetimes, is less than 30%, as the decay time in the waiting-time dependence is much slower than the rise time (Figure 3). By the same reason the overall cooling time will not affect much the γ values. Therefore, the likely reason for larger γ in *o*-AcPhCN comes from the presence of efficient relaxation pathways populating the modes coupled strongly to the CO mode. The CO coupling pattern, however, is similar in all three isomers in many respects; for example, the two modes that are coupled most strongly to the CO are of the same nature in all three isomers (vide infra). Despite the largest γ, the CO mode in the ortho isomer is coupled weaker, in average, to other modes in comparison to that in the meta and para isomers (Table 3). Therefore, existence of the relaxation pathways populating efficiently the modes that are strongly coupled to the CO mode in the ortho but not in meta and para isomers is likely the main reason for large γ in *o*-AcPhCN. Note that the higher frequency modes loose energy faster than the lower frequency modes as the latter have a better chance to be repopulated again from the excess energy present in the molecule. The high-frequency modes, therefore, can substantially contribute to the cross peak only at small time delays.

Expectedly, a group of modes at the acetyl moiety are coupled strongest to the CO mode and some of them have relatively high frequencies around 1000 cm^{-1} (Table 3). Two modes involving methyl group rocking and CC stretching motions bare the largest anharmonicity with CO, are found for mode #21 at 953.6 cm^{-1}

($\Delta_{CO/\#21} = -4.14$ cm^{-1}) and for mode #24 at 1020.6 cm^{-1} ($\Delta_{CO/\#24} = -2.12$ cm^{-1}). One can estimate how much these modes have to be populated (δn_j) to cause $\gamma \approx 10$ using a linear relation between the cross peak amplitude ($F(T)$) and the anharmonicity applicable when the anharmonicity is much smaller than the width of the transitions:[46,47] $F(T) = a\Sigma_j \Delta_{CO/j}\delta n_j$ and $F(0) = a\Delta_{CN/CO}\delta n_{CN}$, where a is the proportionality constant, $\delta n_j(T) = n_j(T) - n_j^{eq}$, $n_j(T)$, and n_j^{eq} are the j-mode populations at the waiting time T and at room temperature thermal equilibrium, respectively, and summation should be taken over all modes in the molecule populated excessively compared to their thermal population. The amplification factor γ is given by the following ratio:

$$\gamma = \frac{F(T_{max})}{F(0)} = \frac{1}{\Delta_{CN/CO}} \sum_j \Delta_{CO/j} \frac{\delta n_j(T_{max})}{\delta n_{CN}} \quad (1)$$

For example, about a 10-fold amplification factor is achieved if a mode #21 alone is populated to $\delta n_{\#21} \approx 0.11$ via IVR ($\gamma = -4.14/(-0.047)0.11 \approx 10$). It requires ca. 24% population of a mode j with $\Delta_{CO/j}$ of about 2 cm^{-1} to get $\gamma \approx 10$. There are many other modes in the molecule that, despite having a smaller coupling with CO, are populated substantially via IVR. It is expected that the modes #21 and #24 are contributing significantly at T_{max}, especially in *o*-AcPhCN; it is unclear if these modes are populated efficiently directly from CN relaxation or more relaxation steps are needed to excite them. The essentially instantaneous rising time of the deconvoluted function for o-AcPhCN (Figure 6) suggests a possibility of direct CN relaxation into one or both of these modes, but modeling shows that it is not the case and other modes have larger contribution at delays smaller than 2 ps (vide infra). Note that the frequencies of modes #21 and #24 are about half of the frequency of the CN mode; such high-frequency modes are expected to decay rapidly in molecules with large density of states and in the meta and para isomers they are just too far spatially from the CN group to be excited efficiently, which is the expected reason for smaller γ there.

The modes in the 300−1000 cm^{-1} frequency range are coupled to the CO mode similarly, in average, in all three isomers (Table 3). As the energy dissipation progresses, only the low-frequency modes remain excited excessively. Interestingly, the modes with frequencies less than 300 cm^{-1} in *o*-AcPhCN are coupled substantially weaker to the CO mode, compared to that in the meta and para isomers (Table 3). Drastic decrease of the cross-peak amplitude is expected in *o*-AcPhCN when the modes with frequencies higher than ca. 450 cm^{-1} relax, as oppose to *m*- and *p*-AcPhCN where the coupling of the low-frequency modes to CO is substantial. Indeed, the cross peak amplitude decays much faster in *o*-AcPhCN than in *m*- and *p*-AcPhCN and essentially reaches zero already at ca. 30 ps (Figure 3a). In contrast, in the meta and para isomers there are lower-frequency modes (147 and 608 cm^{-1} in meta and 158 and 538 cm^{-1} in para) having the anharmonicities with CO larger than 2.2 cm^{-1} (Table 3). These modes stay excited longer and are expected to contribute most to the cross peak at $T \geq T_{max}$ in *m*- and *p*-AcPhCN. Certainly, the presence of low-frequency modes coupled strongly to CO is the main reason of much longer decay of the CN/CO cross peak in *m*- and *p*-AcPhCN (Table 3, <300 cm^{-1}, Figure 4b,c).

Note that the cross-peak decay ($T > T_{max}$) is often assigned to the overall cooling time of the molecule to the solvent. The data

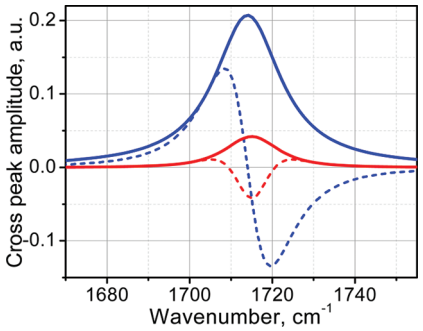

Figure 7. Two CN/CO computed cross-peak ω_t spectra are shown; each includes the real-part spectrum (dashed line) and the magnitude spectrum (solid line). The first spectrum (blue) includes two transitions, $|0\rangle \rightarrow |CO\rangle$ and $|X\rangle \rightarrow |X + CO\rangle$, where $\Delta_{CO/X} = -2$ cm^{-1}. The second spectrum (red) in addition includes a transition $|Y\rangle \rightarrow |Y + CO\rangle$, where $\Delta_{CO/Y} = +2$ cm^{-1} and the states $|X\rangle$ and $|Y\rangle$ are equally populated. The second spectrum is ca. 5 fold weaker than the first, illustrating the cancellation effect in the cross peaks when two states are present with positive and negative CO anharmonicities.

obtained for the ortho isomer show that care should be taken in such assignments as it is possible to have very small contribution to cross-peaks from the low-frequency modes, which makes the cooling look faster than it actually is. In this case the cross peak decay represents only the cooling of the relatively high frequency modes, but not the overall cooling of the molecule.

The mean anharmonicity of the low-frequency modes (<300 cm^{-1}) with the CO mode in *o*-AcPhCN is small mostly due to a compensation of the negative and positive anharmonicities, although the mean absolute-value anharmonicity is also ca. 1.7 times smaller than those in *m*- and *p*- AcPhCN (Table 3). While most of the anharmonicities are negative, shifting the respective combination band level to lower frequencies, there are a few anharmonicities that are positive (Table S1). Importantly, if the mean anharmonicity is reduced due to the cancellation of positive and negative contributions, the cross-peak amplitude is severely reduced as well. Figure 7 shows a modeling illustrating such reduction of the cross-peak amplitude. Real and absolute part spectra were computed for two cases. In the first case the cross peak originated from populating a mode X having $\Delta_{CO/X} = -2$ cm^{-1} (blue lines, solid for magnitude spectrum and dashed for the real part spectrum) and in the second the cross peak originated from populating equally two modes, X and Y, so that $\Delta_{CO/X} = -2$ cm^{-1} and $\Delta_{CO/Y} = +2$ cm^{-1} (red lines). Note that equal populations of modes X and Y result in the maximal cancellation of the two contributions. Indeed, the maximum of the second signal (magnitude spectrum) is ca. 5 fold smaller than that of the first signal. The cancellation depends linearly on the $\Delta_{CO/X}$ and $\Delta_{CO/Y}$ values;[46,48] ca. 10-fold signal suppression occurs if they are ca. $\pm$ 1 cm^{-1}. At the waiting times of several tens of picoseconds the populations of the vibrational modes of AcPhCN are expected to be close to a thermal equilibrium.[47] Assuming such equilibrium, one can calculate a mean frequency shift for the CO mode caused by the temperature increase: $\Delta\nu_{temp} = \langle\Delta_{CO/i}\rangle_{thermal} = \sum_{i=1}^{3N-6} \Delta n_i \Delta_{CO/i}$, where $\Delta n_i = n_i(\text{Temp}) - n_i(\text{Temp}_{room})$ is an increase of the thermal population of mode i due to the temperature increase with n_i equals $n_i(\text{Temp}) = (e^{h\nu_i/k_B\text{Temp}} - 1)^{-1}$. The results ($\Delta\nu_{temp}$), calculated in Table 3 for a temperature increase of 10 K with respect to the room temperature, show the same tendency as the mean

anharmonicities: the shift for the ortho isomer is 2 and 2.5 times smaller than those for the meta- and para isomers, respectively. Theoretical modeling shows a further proof that the small mean CO/X anharmonicity for the low-frequency modes in *o*-AcPhCN is the cause for the faster decay of its cross peak amplitude at $T > T_{max}$.

Modeling of Vibrational Relaxation and Energy Transport. A recently developed theoretical model[36] that is based on generalization of Marcus electron transfer theory to anharmonic transitions[49] was used to describe vibrational relaxation and intramolecular vibrational energy redistribution (IVR) processes in the three isomers. The nonequilibrium time-dependent populations of the vibrational modes were found within the collision integral formalism of ref 36 and using the X-matrix of anharmonic couplings determined from the DFT calculations with the Gaussian 09 suite.[33] The overall cooling to the solvent was treated in the rate equation approximation assuming that all modes of the solute have the same equilibration time due to their coupling to the solvent, which was taken to be 14 ps. Compared to the formulation in ref ·, several modifications were made to the theory, which will be presented in detail in a separate publication. Briefly, anharmonic transition rates have been calculated by extending the nonadiabatic expression for the electron transfer reaction rate derived by Bixon and Jortner[50] to anharmonic transitions. Only third-order anharmonicities has been considered. Similarly to the earlier work[36] the transition involving three modes a, b, c (n_a, n_b, $n_c \rightarrow n_a - 1$, $n_b + 1$, $n_c + 1$) is induced by the anharmonic interaction of all three modes with low frequency vibrations, d, $(V_{aad} - V_{bbd} - V_{ccd})(b_d^+ + b_d)$, where V_{iij} is the third-order derivative of the potential energy and b_d^+ and b_d are the raising and lowering operators, respectively. The reorganization energy is determined from the mean squared fluctuations of the transition with the cutoff of high frequency mode contributions by the Boltzmann factor, similarly to that described in ref ·, while the matrix element V_{abc} determined the energy transfer amplitude. In contrast to the previous work,[36] the preexponential factor for the adiabatic regime has been estimated following the classical Holstein work.[51] It turns out that in all cases of interest the transitions occur in a nonadiabatic manner, so the Fermi Golden rule expression from ref 52 was sufficiently accurate. The lifetimes of the excited vibrational modes and the time evolution of their populations following the excitation of the CN stretching vibration have been studied using the same collision integral approach as in refs 36 and 53.

The simulated lifetimes of the CN stretching mode for the three isomers were found at 1.2, 3.8, and 3.4 ps for the ortho, meta, and para isomers, respectively, compared to the experimental values of 3.4, 7.1, and 7.2 ps (Table 2). We consider this agreement to be reasonable, as a similar trend is found. The CO mode excited state lifetimes were calculated at 1.05, 1.9, and 2.0 ps, which also match well the experimental values of 1.8, 1.2, and 2.1 ps, found for *o*-, *m*-, and *p*-AcPhCN, respectively. Although such good prediction for the lifetimes in all three compounds is encouraging, the waiting-time dependence modeling for the for the cross-peak amplitude are much more demanding as they require accurate computation of all IVR channels in the molecule.

The computed time-dependent mode populations $(n_j(T))$ were used to reconstruct the waiting time dependence of the CN/CO cross peaks. The mean frequency shift of the CO mode induced by excessive population of a mode j is given by $\delta n_j(T)\Delta_{CO/j}$. The cross-peak contribution of mode j can be

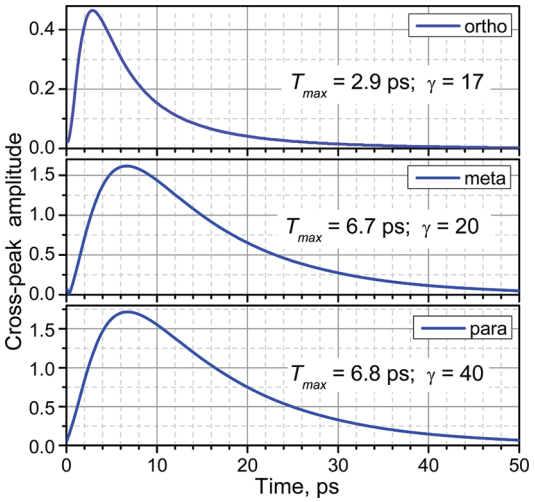

Figure 8. Modeled CN/CO cross-peak amplitudes as a function of the waiting time, T, for the ortho, meta, and para isomers. The following values were used for the modeling $\Gamma = 10$ cm^{-1} and $\sigma = 23$ cm^{-1}. The lowest frequency mode for the ortho isomer was eliminated by setting $\Delta_{CO/\#1}$ to zero (see also Figure S2). We have also computed the dynamics if the cutoff frequency is raised to 60 cm^{-1}, so that the lowest frequency modes are eliminated in the meta and para isomers as well. The dynamics for the meta and para isomers do not change substantially with the respective amplification factors of 19.7 and 40 and the T_{max} values of 7.3 and 6.9 ps.

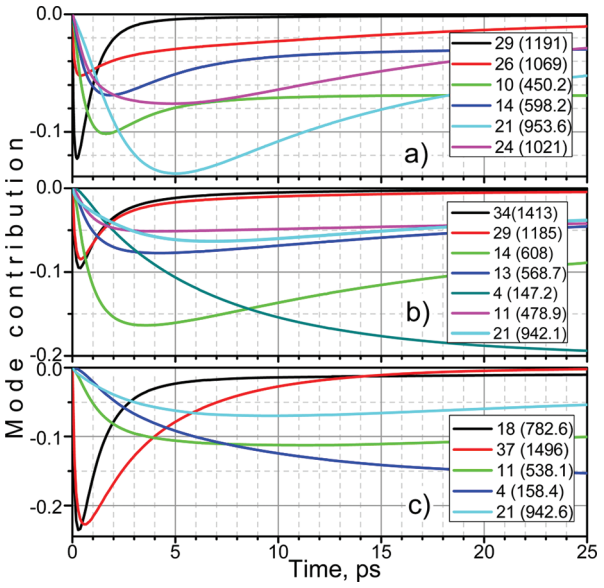

Figure 9. Contributions to the CN/CO cross peak, $P_j(T)$, for selected modes for a) *o*-, (b) *m*-, and (c) *p*-AcPhCN. The modes are indicated by the mode number and the frequency (in parentheses), see inset.

described in the time domain as $M_j(t,T) = \exp[-i(\omega_{CO} + \Delta_{CO/j})t - \Gamma t - 0.5\sigma^2 t^2] - \exp[-i\omega_{CO}t - \Gamma t - 0.5\sigma^2 t^2]$, where Γ and σ are homogeneous and inhomogeneous width contributions to the CO stretching. To take into account a larger transition dipole of the $|1\rangle \rightarrow |2\rangle$ CO transition (taken as $\mu_{1\rightarrow 2} = \sqrt{2}\mu_{0\rightarrow 1}$) and the presence of the stimulated emission[38] the contribution from the CO diagonal signal was doubled, $M_{All}(t,T) = \Sigma_{j\neq CO} n_j M_j(t,T) + 2n_{CO}M_{CO}(t,T)$. The signal in the frequency

dx.doi.org/10.1021/jp2066315 |J. Phys. Chem. B 2011, 115, 11063–11073

domain is obtained by a Fourier transformation, $S(\omega,T) = FFT\{M_{All}(t,T)\}$; a maximum of the abs($S(\omega,T)$) function was determined at each waiting time and plotted in Figure 8.

The computed energy transport times, T_{max}, found at 2.9, 6.7, and 6.8 ps for the ortho, meta, and para isomers, respectively, reproduce reasonably the experimental trend. The computed amplification factors, however, deviate substantially from the experiment (Table 3). While γ is closely reproduced for the ortho isomer, it is strongly overestimated for the meta and para isomers. The decay tails of the computed curves show the same trend as in the experiment; that is, the tail for the ortho isomer decays much faster than the tails for the meta- and para- isomers. Note that the same overall cooling time of 14 ps was used for all three compounds.

To get an insight into the relaxation process the relative cross-peak contributions from various modes were analyzed. The quantity, $P_j(T) = [(n_j(T) - n_j^{eq})\Delta_{CO/j}]/[\Sigma_{j=1,...,48}(n_j(T) - n_j^{eq})\Delta_{CO/j}]$, where the summation is performed over all modes in the molecules, represents the relative cross-peak contribution fractions from mode j. The $P_j(T)$ time dependences for several modes that contribute the most to the cross peak at different time intervals are plotted in Figure 9. For example, in the ortho compound modes #29 (1191 cm^{-1}) and #26 (1069 cm^{-1}) contributions reach maximum at ca. 0.3−0.4 ps; along with the modes #37 (1475.8 cm^{-1}) and #27 (1115.7 cm^{-1}) these modes are the largest contributors at early time delays. All of these modes, while highly delocalized, involve the NC-Ph bond stretching or bending motion. They all have relatively high frequencies, which results in their fast depopulation. For the next tier of modes peak at ca. 1.5 ps, the largest contribution comes from modes #10, #14, and #13, which have frequencies of 450−605 cm^{-1}, and although also highly delocalized, all involve C−CO−C bending motion at the acetyl group, which ensures their substantial coupling to the CO stretching mode (Table S1). The CO stretching mode gets excited slightly in *o*-AcPhCN ($\delta n_{CO}(T_{max})$ = 0.0048) which contributes ca. 25% to the cross-peak amplitude at T_{max} due to its large (diagonal) anharmonicity. The next tier of modes peaks at ca. 4.5 ps; the largest contributors here are modes #21 and #24, which are more localized at the acetyl group, both having a substantial CH_3 group rocking (bending) contribution. The largest contributions at T_{max} = 2.9 ps in *o*-AcPhCN come from modes #21 (12%), #40(12%), #10 (10%), #24 (7.5%), #14 (7%), and #13 (5%).

Similar behavior is found in the meta- and para- isomers, only the time scales are slightly different (Figure 9). The modes contributing most at early time delays peak at 0.3−0.6 ps in *m*-AcPhCN (#34, #29, #30, and #39) and in *p*-AcPhCN (#18, #37, #15, and #26) have all relatively high frequencies (Table S1). The next tier of modes peaking at 2.5−3 ps in *m*-AcPhCN (#14, #13, #25, and #11) and at ca. 7 ps in *p*-AcPhCN (#11), has lower frequencies and substantial presence at the acetyl moiety. The cross-peak contributions of the CO stretching mode excitation in the meta and para isomers are also substantial amounting at 7% and 15% at their respective T_{max} with $\delta n_{CO}^{meta}(6.7\ ps)$ = 0.0035, $\delta n_{CO}^{para}(6.8\ ps)$ = 0.0073. The modes contributing most at T_{max} = 6.7 ps in *m*-AcPhCN include modes #4 (27%), #14 (12.5%), #40 (7%), #13 (6%), #21 (5%), #11 (4.5%), and #25 (4%). The largest contributors in *p*-AcPhCN at T_{max} = 6.9 ps include modes #40 (15%), #11 (11.5%), #4 (11.5%), #21 (7%), #6 (7%), and #14 (5%) (Figure 9).

The modeling predicts that modes #21 and #24(#25 in m- and p-AcPhCN) are not populated directly from CN, even in the ortho isomer; the mean number of steps needed for their efficient population increases with an increase of the distance between the CN and CO groups. Satisfyingly, the model describes well the faster decay of the cross peak for *o*-AcPhCN at $T > T_{max}$.

The discrepancies between the modeling and experiment, most notably in the amplification factors, can be attributed to a variety of reasons, including insufficiently accurate description of vibrational transitions using DFT anharmonic calculations, inadequate description of interaction with the solvent, and exclusion of the higher-order relaxation pathways. For example, there is a clear indication that for the ortho isomer the anharmonicity among CO and the lowest-frequency mode ($\Delta_{CO/\#1}$ = 0.65 cm^{-1}) and/or its frequency ($\omega_{\#1}$ = 29.5 cm^{-1}) are incorrectly evaluated. The lowest frequency mode corresponds to a deformation motion involving essentially all atoms of the molecule. For the computed waiting-time dependence (Figure 8) a cutoff frequency of 30 cm^{-1} has been introduced by setting to zero the anharmonicities with CO for all modes below the cutoff frequency. The results obtained without a cutoff deviates qualitatively from the experiment for the ortho isomer (Figure S2). An increase in the cutoff frequency to 60 cm^{-1}, resulting in elimination of one mode for each isomer, does not change much the modeling curves for the meta and para isomers (see Figure 8 caption).

Out of all vibrational modes computed with Gaussian 09 for AcPhCN in the gas phase, the lowest frequency modes are expected to be the least transferrable to describe the molecule in solution. Unfortunately, the DFT calculations for a molecule in solution with the solvent described with a polarizable continuous model produced imaginary anharmonic frequencies for the lowest frequency modes and could not therefore be used in the modeling. In general, the theoretical model developed is expected to be rather sensitive to the values of the frequencies and couplings of the low-frequency modes for describing correctly the relaxation pathways. The ability of describing the main features of the waiting time dependence for all three isomers suggests that the majority of the frequencies and the anharmonic constants are reasonable and useful for describing the energy transport in molecules. Nevertheless, the theory has to be tested further and could be expanded to include fourth-order interactions in the Hamiltonian, quantum description of molecular states, more sophisticated cooling mechanism to the solvent, and better determination of the anharmonic frequencies and anharmonic constants for a molecule in a solvent.

CONCLUSIONS

The molecular level energy transport in the ortho, meta, and para isomers of acetylbenzonitrile has been studied using the methods of 2DIR spectroscopy. The results clearly show a correlation between the energy transport time and the intermode distance. They also suggest that the vibrational modes of the phenyl ring are not fully delocalized on the ring and that the acetyl and cyano group substitutions strongly perturb the delocalization. It is shown that the cross peak decay occurring at the waiting-time delays $T > T_{max}$, which was often associated with the overall cooling of the compound to the solvent, may indicate the cooling of only modes in a particular frequency range, as in the case for the *o*-AcPhCN isomer where a very small CN/CO cross peak is found even when the low-frequency modes are excessively excited. The vibrational relaxation and the energy transport dynamics have been modeled theoretically using a Marcus type approach applied to anharmonic transitions. Using solely the third-order relaxation pathways, the modeling is

capable of reproducing well most of the characteristic features of the experiment that include the lifetimes of the excited modes (CN and CO stretching), energy transport times (T_{max}), and overall cooling of the molecule for all three isomers studied.

■ ASSOCIATED CONTENT

Supporting Information. Included are diagonal CO and CN transient spectra for meta and para isomers, cross-peak modeling for *o*-AcPhCN performed with mode #1, normal mode displacement vectors for selected modes, and the table of anharmonic frequencies and anharmonic constants for all three isomers. This material is available free of charge via the Internet at http://pubs.acs.org.

■ AUTHOR INFORMATION

Corresponding Author
*E-mail: irubtsov@tulane.edu.

■ ACKNOWLEDGMENT

Support by the National Science Foundation (CHE-0750415 and CHE-0936133 to I.V.R. and CHE-0628092 to A.L.B.) is gratefully acknowledged. V.M.K. is thankful for the fellowship from the IBM Corporation.

■ REFERENCES

(1) Elsaesser, T.; Kaiser, W. *Annu. Rev. Phys. Chem.* **1991**, *42*, 83.
(2) Fujisaki, H.; Straub, J. E. *Proc. Natl. Acad. Sci. U.S.A.* **2005**, *102*, 6726.
(3) Gruebele, M.; Wolynes, P. G. *Acc. Chem. Res.* **2004**, *37*, 261.
(4) Leitner, D. M. *Adv. Chem. Phys.* **2005**, *130 B*, 205.
(5) Deak, J. C.; Iwaki, L. K.; Rhea, S. T. *J. Raman Spectrosc.* **2000**, *31*, 263.
(6) Pein, B. C.; Seong, N.; Dlott, D. D. *J. Phys. Chem. A* **2010**, *114*, 10500.
(7) Seong, N.-H.; Fang, Y.; Dlott, D. D. *J. Phys. Chem. A* **2009**, *113*, 1445.
(8) Fang, Y.; Shigeto, S.; Seong, N.-H.; Dlott, D. D. *J. Chem. Phys.* **2009**, *113*, 74.
(9) Backus, E. H. G.; Nguyen, P. H.; Botan, V.; Moretto, A.; Crisma, M.; Toniolo, C.; Zerbe, O.; Stock, G.; Hamm, P. *J. Phys. Chem. B* **2008**, *112*, 15487.
(10) Hamm, P.; Ohline, S. M.; Zinth, W. *J. Chem. Phys.* **1997**, *106*, 519.
(11) Hirai, S.; Banno, M.; Ohta, K.; Palit, D.; Tominaga, K. *Chem. Lett.* **2010**, *39*, 932.
(12) Nagele, T.; Hoche, R.; Zinth, W.; Wachtveit, J. *Chem. Phys. Lett.* **1997**, *272*, 489.
(13) Kurochkin, D. V.; Naraharisetty, S. G.; Rubtsov, I. V. *Proc. Natl. Acad. Sci. U.S.A.* **2007**, *104*, 14209.
(14) Rubtsov, I. V. *Acc. Chem. Res.* **2009**, *42*, 1385.
(15) Hamm, P.; Lim, M.; Hochstrasser, R. M. *J. Phys. Chem. B* **1998**, *102*, 6123.
(16) Hochstrasser, R. M. *Chem. Phys.* **2001**, *266*, 273.
(17) Asbury, J. B.; Steinel, T.; Fayer, M. D. *J. Luminesc.* **2004**, *107*, 271.
(18) Demirdoeven, N.; Cheatum, C. M.; Chung, H. S.; Khalil, M.; Knoester, J.; Tokmakoff, A. *J. Am. Chem. Soc.* **2004**, *126*, 7981.
(19) Strasfeld, D. B.; Ling, Y. L.; Shim, S.-H.; Zanni, M. T. *J. Am. Chem. Soc.* **2008**, *130*, 6698.
(20) Maekawa, H.; Ballano, G.; Toniolo, C.; Ge, N.-H. *J. Phys. Chem. B* **2011**, *115*, 5168.
(21) Garrett-Roe, S.; Hamm, P. *J. Chem. Phys.* **2009**, *130*, 164510/1.
(22) Kasyanenko, V. M.; Lin, Z.; Rubtsov, G. I.; Donahue, J. P.; Rubtsov, I. V. *J. Chem. Phys.* **2009**, *131*, 154508.
(23) Naraharisetty, S. G.; Kasyanenko, V. M.; Rubtsov, I. V. *J. Chem. Phys.* **2008**, *128*, 104502.
(24) Baev, A.; Rubio-Pons, O.; Gel'mukhanov, F.; Agren, H. *J. Phys. Chem. A* **2004**, *108*, 7406.
(25) Galperin, M.; Ratner, M.; Nitzan, A. *J. Phys. Condensed Matter* **2007**, *19*, 103201/1.
(26) Graetzel, M. *Inorg. Chem.* **2005**, *44*, 6841.
(27) Lin, Z.; Lawrence, C. M.; Xiao, D.; Kireev, V. V.; Skourtis, S. S.; Sessler, J. L.; Beratan, D. N.; Rubtsov, I. V. *J. Am. Chem. Soc.* **2009**, *131*, 18060.
(28) Bloem, R.; Dijkstra, A. G.; Jansen, T. L.; Knoester, J. *J. Chem. Phys.* **2008**, *129*, 055101/1.
(29) Didraga, C.; Malyshev, V. A.; Knoester, J. *J. Phys. Chem.* **2006**, *110*, 18818.
(30) Kenkre, V. M.; Tokmakoff, A.; Fayer, M. D. *J. Chem. Phys.* **1994**, *101*, 10618.
(31) Yu, X.; Leitner, D. M. *J. Phys. Chem.* **2003**, *107*, 1698.
(32) Yu, X.; Leitner, D. M. *J. Chem. Phys.* **2005**, *122*, 054902.
(33) Barone, V. *J. Chem. Phys.* **2005**, *122*, 014108.
(34) Martin, J. M. L.; Lee, T. J.; Taylor, P. R.; Francois, J. P. *J. Chem. Phys.* **1995**, *103*, 2589.
(35) Hochstrasser, R. M. *Adv. Chem. Phys.* **2006**, *132*, 1.
(36) Burin, A. L.; Tesar, S. L.; Kasyanenko, V. M.; Rubtsov, I. V.; Rubtsov, G. I. *J. Chem. Phys. C* **2010**, *114*, 20510.
(37) Frisch, M. J.; Trucks, G. W.; Schlegel, H. B.; Scuseria, G. E.; Robb, M. A.; Cheeseman, J. R.; Scalmani, G.; Barone, V.; Mennucci, B.; Petersson, G. A.; Nakatsuji, H.; Caricato, M.; Li, X.; Hratchian, H. P.; Izmaylov, A. F.; Bloino, J.; Zheng, G.; Sonnenberg, J. L.; Hada, M.; Ehara, M.; Toyota, K.; Fukuda, R.; Hasegawa, J.; Ishida, M.; Nakajima, T.; Honda, Y.; Kitao, O.; Nakai, H.; Vreven, T.; Montgomery, Jr., J. A.; Peralta, J. E.; Ogliaro, F.; Bearpark, M.; Heyd, J. J.; Brothers, E.; Kudin, K. N.; Staroverov, V. N.; Kobayashi, R.; Normand, J.; Raghavachari, K.; Rendell, A.; Burant, J. C.; Iyengar, S. S.; Tomasi, J.; Cossi, M.; Rega, N.; Millam, N. J.; Klene, M.; Knox, J. E.; Cross, J. B.; Bakken, V.; Adamo, C.; Jaramillo, J.; Gomperts, R.; Stratmann, R. E.; Yazyev, O.; Austin, A. J.; Cammi, R.; Pomelli, C.; Ochterski, J. W.; Martin, R. L.; Morokuma, K.; Zakrzewski, V. G.; Voth, G. A.; Salvador, P.; Dannenberg, J. J.; Dapprich, S.; Daniels, A. D.; Farkas, Ö.; Foresman, J. B.; Ortiz, J. V.; Cioslowski, J.; Fox, D. J. *Gaussian 09*, revision A.02; Gaussian, Inc.: Wallingford, CT, 2009.
(38) Kurochkin, D. V.; Naraharisetty, S. G.; Rubtsov, I. V. *J. Phys. Chem. A* **2005**, *109*, 10799.
(39) Naraharisetty, S. G.; Kurochkin, D. V.; Rubtsov, I. V. *Chem. Phys. Lett.* **2007**, *437*, 262.
(40) Lian, T.; Locke, B.; Kholodenko, Y.; Hochstrasser, R. M. *J. Phys. Chem.* **1994**, *98*, 11648.
(41) Wang, Z.; Pakoulev, A.; Dlott, D. D. *Science* **2002**, *296*, 2201.
(42) Naraharisetty, S. R. G.; Kasyanenko, V. M.; Zimmermann, J.; Thielges, M. C.; Romesberg, F. E.; Rubtsov, I. V. *J. Phys. Chem. B* **2009**, *113*, 4940.
(43) Rubtsov, I. V.; Naraharisetty, S. G.; Keating, C.; McClure, B. A.; Rack, J. J.; Kasyanenko, V. M. Relaxation-assisted dual-frequency two-dimensional infrared spectroscopy: measuring distances and bond connectivity. In *Springer Series in Chemical Physics*; Corkum, S. D. S., Nelson, K., Ed.; Springer: New York, 2009; Vol. 92, pp 400.
(44) Deak, J. C.; Pang, Y.; Sechler, T. D.; Wang, Z.; Dlott, D. D. *Science* **2004**, *306*, 473.
(45) Schade, M.; Hamm, P. *J. Chem. Phys.* **2009**, *131*, 044511/1.
(46) Rubtsov, I. V.; Hochstrasser, R. M. *J. Phys. Chem. B* **2002**, *106*, 9165.
(47) Lin, Z.; Keiffer, P.; Rubtsov, I. V. *J. Phys. Chem. B* **2011**, *115*, 5347.
(48) Keating, C. S.; McClure, B. A.; Rack, J. J.; Rubtsov, I. V. *J. Chem. Phys.* **2010**, *133*, 144513/1.
(49) Rips, I.; Jortner, J. *J. Chem. Phys.* **1987**, *87*, 2090.
(50) Bixon, M.; Jortner, J. *J. Phys. Chem.* **1981**, *85*, 3759.

(51) Holstein, T. *Ann. Phys.* **1959**, *8*, 343.
(52) Buhks, E.; Bixon, M.; Jortner, J.; Navon, G. *J. Phys. Chem.* **1981**, *85*, 3759.
(53) Stuchebrukhov, A. A.; Kuz'min, M. V.; Bagratashvili, V. N.; Letokhov, V. S. *Chem. Phys.* **1986**, *107*, 429.